Dosimetric Model for Locoregional Treatments of Brain Tumors with ^{90}Y-Conjugates: Clinical Application with ^{90}Y-DOTATOC

Mahila Ferrari, PhD[1,2]; Marta Cremonesi, PhD[1,2]; Mirco Bartolomei, MD[1]; Lisa Bodei, MD[1]; Marco Chinol, PhD[1]; Maurizio Fiorenza, CTSRM[1]; Giampiero Tosi, PhD[2]; and Giovanni Paganelli, MD[1]

[1]Division of Nuclear Medicine, European Institute of Oncology, Milan, Italy; and [2]Medical Physics, European Institute of Oncology, Milan, Italy

Locoregional (LR) administration of ^{90}Y-conjugates after surgical debulking is a promising therapeutic option of gliomas. Dosimetry is highly recommended, as patient-specific parameters influence the absorbed dose to target and normal tissues. After tumor resection, the absorbed dose must be carefully evaluated in the rim of tissue surrounding the resected area. The aim of this study was to calculate and provide the S values, according to the MIRD concept, for dosimetry of LR brain treatments with several ^{90}Y-labeled compounds. The S values thus obtained have been clinically applied in 12 patients treated with ^{90}Y-labeled [DOTA^0,D-Phe^1,Tyr^3]octreotide (^{90}Y-DOTATOC). **Methods:** An anthropomorphic model for Monte Carlo simulations was developed to evaluate absorbed doses in brain-adjacent tissue (BAT) and in normal brain. To adapt the model to single patients, S values were evaluated taking into account (i) different surgical resection cavity (SRC) volumes, (ii) different percentages of conjugate binding to the cavity wall, and (iii) different depths of percolation of the conjugate trough the cavity wall. BAT was divided into 1-mm-thick consecutive adjacent shells to evaluate the dose distribution around the cavity. Corresponding S values were obtained to allow dosimetric evaluation in brain LR therapy with ^{90}Y-conjugates. In the clinical treatments, 0.4–1.1 GBq of ^{90}Y-DOTATOC were injected into the SRC via an appropriate catheter. The activity in the SRC was assumed to be the difference between the total injected activity and the activity in the blood plus the activity cumulatively eliminated with the urine. **Results:** Assuming no diffusion, with a mean residence time in SRC of 60 ± 8 h, absorbed doses to shell II were 0.25 and 0.03 Gy/MBq for SRC volumes of 7.2 and 65.4 mL, respectively. Assuming a slight diffusion of 1 mm with a 7.2-mL SRC, absorbed dose to shells I, II, and VI were consistently different: 5.32, 2.53, and 0.12 Gy/MBq, respectively. Mean doses to normal brain, red marrow, bladder wall, and total body were 0.015, 0.03, 1.22, and 0.006 MGy/MBq. **Conclusion:** The model proved to be suitable for the dosimetry of several LR therapies with ^{90}Y-conjugates. According to our results, LR treatment with ^{90}Y-DOTATOC can safely deliver very high doses to target tissue, sparing normal organs including brain.

Malignant gliomas are refractory to conventional treatments. Protocols including aggressive combined therapies, such as surgical debulking, external beam radiotherapy (EBRT) and chemotherapy, usually provide time-limited results, and local recurrence is a common event occurring in a few months (*1*). Surgical resection represents the only curative option, but it is practically impossible to remove the microscopic disease spreading into the brain-adjacent tissue (BAT; ranging from 1 to 3 cm in depth), which gives rise to the recurrence (*2*). The efficacy of conventional external radiotherapy has been demonstrated (*3*), but no more than 60 Gy can be delivered, because of unacceptable risks of neurologic toxicity.

Therefore, both systemic and locoregional (LR) radionuclide therapies have been developed, especially in recurrent disease, to improve survival (*4*) by increasing the local boost to the target. Compared with systemic treatment, local administration has been demonstrated to be advantageous (*5*), bypassing the blood–brain barrier, thus allowing high local activity concentrations and the reduction of systemic toxicity.

Among the radionuclides used in clinical practice, ^{90}Y has physical and radiobiologic features suitable for a LR approach, due to its high-energy β^--particles (maximum energy, 2.28 MeV). Moreover, ^{90}Y penetration (maximum particle range in tissue, 12 mm; range in tissue after which 50% of the energy particles is transferred, 4 mm) allows high radiation doses to the target area, while sparing surrounding tissues and normal organs and maximizing the tumor-to-nontumor dose ratio.

Different radiolabeled compounds have been proposed for LR treatment (*6–10*), mainly antitenascin monoclonal antibodies overexpressed in the matrix of high-grade gliomas (*11*), and somatostatin analogs recognizing sst2–sst5 receptors (sstr2–sstr5) (*12*). These molecules are used to transport the radioactivity to the tumor cells.

After injection into the surgical resection cavity (SRC), the radiocompound, monoclonal antibody, or peptide either diffuses into the BAT to target the neoplastic cells scattered throughout this region or remains localized in the cavity, depending on tumor cell distribution and on the amount of binding to the tumor cells (13). In the BAT, tumor cells may be hit directly or by the crossfire of β-particles.

The principal aim of the present study was to calculate radiation dose estimates, according to the MIRD formalism (14,15), for ^{90}Y-labeled compounds injected into a brain neocavity, after surgery. In particular, we aimed at estimating the dose to the rim of tissue surrounding the SRC, considering different radiopharmaceutical distributions. Furthermore, we applied the model for dosimetric evaluation, performed on an individual basis, in patients affected by anaplastic astrocytoma, previously submitted to LR receptor radionuclide therapy with ^{90}Y-labeled [DOTA^0,D-Phe^1,Tyr^3]octreotide (^{90}Y-DOTATOC).

MATERIALS AND METHODS

We developed an anthropomorphic computational brain phantom appropriate for the assessment of the dose distribution around the SRC, according to the MIRD method. We calculated the specific absorbed fraction for each defined source–target region applying Monte Carlo procedures. Subsequently, the obtained S values were clinically applied to evaluate the absorbed doses in a group of patients treated with LR application of ^{90}Y-DOTATOC.

Monte Carlo Code

The FLUKA code (16), which simulates photon and electron transport, including the bremsstrahlung contribution, was used to score energy deposition within the tissue. For every defined source region, the FLUKA code was run 5 times, using 10^6 particle histories each time. Particles were randomly generated, assigning directions and positions within each source region, under the assumption of a uniform distribution of the radiopharmaceutical in the source region. The initial energy of the particles was obtained from the ^{90}Y-emission spectrum published in ICRU Report 57 (17).

Phantom

The different areas of the computational phantom involved in the energy deposition were the tumor area (SRC and BAT, as described below), the eyes, the optical nerve, the skull, and the normal brain. The dimensions of eyes and skull were set following ICRP Publication 23 (18) and ICRU Report 48 (19); the distances between different regions were obtained from CT images of patients and phantoms (20). The volume of the brain was set equal to the

volume delimited by the skull; Reference Man values reported in ICRP Publication 23 (18) were assumed for the composition of the brain (Table 1). Two water-equivalent spheres (radium, 1.2 cm) represented the eyes. The skull was modeled combining different elementary geometric solids (ellipsoids, spheres, cones, and frustums of cone). SRCs were assumed to be spheric, with a smooth rigid edge. Homogeneous density of tumor and normal brain tissue (Table 1) were considered, as well as uniform distribution of the radiocompound within any source region. To score energy deposition, the target tissue surrounding the cavity (BAT) was divided in adjacent concentric shells. The inner shells from I to VI, at increasing distances from the center of the cavity, were 1-mm thick. The outer shells were 2-mm thick (Fig. 1).

To evaluate the absorbed dose in the normal brain, tissue farther than 12 mm from the cavity interface was considered as normal brain, in all cases. The value of 12 mm corresponds to the maximum range of ^{90}Y β$^-$-particles.

For simulation purposes, the position of the cavity inside the brain was established on the basis of a typical site of appearance of the tumor considered in this study (glioma) (21). The cavity was considered inside the right brain portion of the head phantom at the same transaxial level of the right eye. The distance between the center of the eye and the center of the cavity was 7 cm. The presence of the Ommaya or Rickam reservoir was not included.

Sources

The model allows calculation of the dose delivered to the BAT for a range of parameters with regard to the cavity and to the radiopharmaceutical distribution inside the cavity and the BAT. The volume of the cavity ranged from 0.5 to 65.4 mL. Once injected, the radiopharmaceutical can distribute uniformly inside the cavity or may be attracted toward the cavity wall. Therefore, we simulated 2 distinct hypotheses (no binding; complete binding). The real situation will probably involve intermediate conditions, in which a fraction, f, of the injected activity localized in a shell immediately surrounding the cavity and a fraction, 1 − f, of injected activity distributed uniformly within the cavity. Moreover, the tumor cell spreading in the BAT can attract the radiopharmaceutical: therefore, the extension of diffusion (d) of the radiopharmaceutical through the cavity wall was also considered. Specifically, the following 2 different situations were modeled:

- Geometry 1: cavity volume varying from 0.5 to 65.4 mL (radius, 0.5–2.5 cm) and different degrees of specific binding factor (f) of the conjugates to the cavity wall:
- Hypothesis 1: no binding (f = 0). All of the activity is uniformly distributed inside the cavity (as in the case of colloids).

TABLE 1
Composition of Different Tissues Expressed as Fractional Elemental Abundance

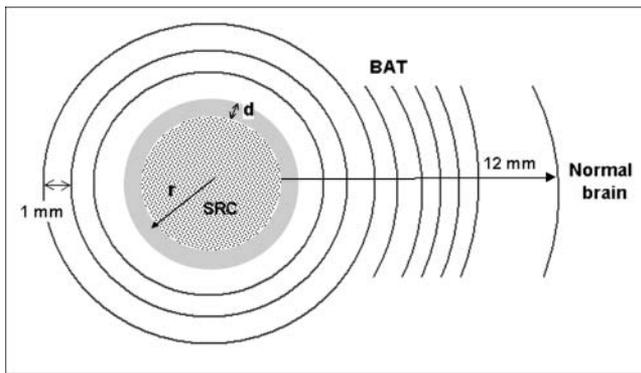| Soft tissue: $\rho = 1.0$ g × cm^{-3}	Skull (bone): $\rho = 1.85$ g × cm^{-3}		Brain: $\rho = 1.03$ g × cm^{-3}		
H = 0.101172	H = 0.063984	Mg = 0.002	H = 0.11	Mg = 0.0015	Na = 0.0018
C = 0.111	C = 0.278	P = 0.07	C = 0.13	P = 0.0035	Cl = 0.0024
N = 0.026	N = 0.027	S = 0.002	N = 0.013	S = 0.0018	K = 0.0031
O = 0.761828	O = 0.410016	Ca = 0.147	O = 0.74	Ca = 0.000089	

ρ = density.

FIGURE 1. BAT model used for Monte Carlo simulation. The different parameters considered are (i) volumes of the cavity, identified by the radium, r; and (ii) percolation of the molecules through the cavity wall, d. Tissue surrounding the cavity was divided in shells 1- or 2-mm thick to score energy deposition. Tissues farther than 12 mm from the cavity wall were considered as normal brain.

- Hypothesis 2: complete binding (f = 1). All of the injected activity is localized in a shell (1-mm thick) immediately surrounding the cavity.
- Geometry 2: cavity volume of 7.2 mL (radium = 1.2 cm, identified as a representative clinical situation) with different depth of diffusion (d) within the BAT. Areas of different thickness—from 1 to 6 mm—surrounding the cavity were considered as sources.

Patients

Twelve patients with recurrent anaplastic astrocytoma (7 males, 5 females; age range, 32–73 y) treated with LR receptor-mediated radionuclide therapy were enrolled in this dosimetric study (Table 2). All patients previously underwent the traditional schedule, including surgical excision, adjuvant EBRT (with a median dose of 60 Gy), and chemotherapy, either in an adjuvant setting (during or immediately after external irradiation) or at recurrence. Patients were required to undergo a second operation to remove or reduce the relapsing tumor and to have an indwelling catheter (connected with a subcutaneous Rickam or Ommaya reservoir) inserted in the SRC, to allow the injection of the radiopharmaceutical.

The main inclusion criteria for the second operation were a Karnofsky performance status of ≥60 and a life expectancy of at least 3 mo. The presence of somatostatin receptors documented by immunohistochemistry was mandatory to enroll the patients for local infusion of ^{90}Y-DOTATOC. Possible acute and delayed side effects induced by the treatment were reported, in terms of hematologic, hepatic, renal, and neurologic toxicity, up to 2 mo after LR therapy.

The study was performed after approval by European Institute of Oncology Ethical Committee. All patients signed informed consent forms after receiving detailed information on the aim and potential risks of the study and agreed to the collection of the data for the dosimetric study.

Reagents

DOTATOC was provided by piCHEM (Austria). ^{90}Y-Cl$_3$ was purchased from PerkinElmer (USA).

DOTATOC (1 μg/μL) in 0.2 mol/L sodium acetate (pH 5.0) was added to 150 μL of 0.4 mol/L sodium acetate/gentisic acid (pH 5.0); this step was followed by the addition of ^{90}Y to achieve a specific activity of 50 GBq/μmol. The mixture was then heated for 30 min at 90°C. Quality control of the products was performed by Sep-Pak C$_{18}$ cartridge (Waters) and by high-performance liquid chromatography as described elsewhere (22). Only a labeling yield exceeding 98% was considered acceptable for injection.

LR Injection and Localization of ^{90}Y-DOTATOC

Patients were hospitalized during the treatment. Under sterile conditions, a volume of 0.5 mL of a defined activity of ^{90}Y-DOTATOC was injected into the SRC, by puncture of the reservoir. Subsequently, the device was gently flushed with 0.5–1 mL of saline. The injected activity ranged between 0.4 and 1.1 GBq. All patients underwent a bremsstrahlung scintigraphic scan 30 min to 1 h after the injection to check the correct localization of ^{90}Y- DOTATOC. Delayed images were then obtained to verify that no washout of radiopharmaceutical from the surgical cavity

TABLE 2
Characteristics of Patients Locoregionally Treated with ^{90}Y-DOTATOC

Patient no.	Age (y)	Sex	Previous treatment	Injected activity ^{90}Y (GBq)	SRC τ (h)	Blood τ (h)	Urine cumulative activity (%)	Urine τ (h)
1	51	M	RT, CH	0.9	68.6	ne	27.2	0.67
2	51	M	RT, CH	1.1	73.2	0.31	23.1	0.73
3	51	M	RT, CH	0.9	59.5	ne	41.6	1.01
4	62	M	RT, CH	1.0	52.5	0.79	47.9	1.13
5	42	F	RT, CH	0.9	58.8	0.49	41.3	0.88
6	41	M	CH	0.6	49.8	0.51	35.8	1.03
7	68	M	CH	0.7	47.7	0.80	53.7	1.3
8	53	F	RT, CH	0.4	70.9	0.38	25.6	0.74
9	32	F	CH	0.5	68.7	0.25	28.8	0.68
10	63	F	CH	0.7	56.7	0.47	47.2	1.29
11	45	M	RT, CH	0.7	59.6	0.52	40.1	1.14
12	73	F	RT, CH	0.7	61.5	0.59	37.4	1.05

ne = not evaluated.

occurred or to control anomalous spreading of ^{90}Y-DOTATOC into the body (Fig. 2).

Pharmacokinetics

To determine the biologic behavior (clearance and rate of excretion) of the radiopharmaceutical, serial blood samples were taken from patients enrolled in the protocol at different time points: 1, 3, 5, 10, 18, 24, 30, 40, and 48 h after the injection of ^{90}Y-DOTATOC. Complete urine collection over 2 d was obtained, with samples collected at 2, 8, 16, 24, 36, and 48 h. Radioactivity measurements, performed on a β-counter, were corrected for physical decay and expressed as the percentage of injected activity (IA) versus time.

To represent the blood clearance of ^{90}Y-DOTATOC, the percentage of IA versus time curve in blood was calculated for each patient by fitting the experimental data to a multiexponential function.

The urinary tract was considered the only route of excretion, as for systemic administration (23). The curve of cumulative activity excreted in the urine versus time was fitted by a biexponential function. The fit parameters were included in the MIRDOSE3.1 software (24) to directly calculate the residence time for urinary bladder contents (τ_{bladd}), considering the dynamic urinary bladder model (25) with a standard voiding interval of 4.8 h (diuresis was not facilitated).

Dosimetry: Normal Organs

The absorbed dose (D) to normal organs was evaluated with the MIRD formalism combining the residence time (τ)—derived from experimental data—and the appropriate S value, by MIRDOSE3.1. As ^{90}Y is a pure β$^-$-emitter, it was difficult to analyze the bremsstrahlung images to accurately quantify the activity distributed in the organism. Therefore, an alternative indirect method to bremsstrahlung imaging was preferred to assess biodistribution. In particular, the residence time in the remainder of the body was set equal to that in the blood (26). The remainder of the body and the urinary bladder residence times were entered into MIRDOSE3.1 to evaluate the absorbed dose to the bladder wall and to the total body. Radiation absorbed dose estimates for bone marrow were derived from the blood activity curve,

FIGURE 2. Anterior and posterior whole-body scintigraphy acquired 16 h after LR therapy with ^{90}Y-DOTATOC. Images are shown with 2 different gray-scale settings. Standard (A) and maximally enhanced (B) demonstrate absence of diffusion of the radiopharmaceutical into other tissues and organs.

considering the same activity concentration for blood and red marrow as suggested for peptides (27).

Dosimetry: Brain and BAT

The absorbed dose to the BAT and to the normal brain was evaluated with the MIRD formalism combining the residence time (τ) of the source—derived from experimental data—and the appropriate S values—calculated by Monte Carlo simulations—as described. The activity in the source versus time was assumed equal to the total injected activity subtracted by the activity in the bloodstream and by the cumulated activity in the urine, at each time point.

RESULTS

S Values

The S values aimed at absorbed dose evaluations of the brain obtained from Monte Carlo simulations are presented in supplemental Appendix A (for target) and supplemental Appendix B (for normal tissues) (available online only at http://jnm.snmjournals.org).

For each cavity volume (from 0.5 to 65.4 mL), the S parameters are reported in case of no binding (geometry 1, hypothesis 1) and in case of complete binding to the BAT (geometry 1, hypothesis 2). In particular, for the cavity volume of 7.2 mL, S values were reported for different penetration, considering the radiopharmaceutical uniformly diffused within a tissue 1- to 6-mm thick (geometry 2).

Pharmacokinetics and Residence Times for ^{90}Y-DOTATOC

Scintigraphic images acquired up to 48 h after the injection of ^{90}Y-DOTATOC showed the radiolabeled compound to be well localized within the injection site and minimal activity in the remainder of the body (Fig. 2). Low ^{90}Y activities were found in the bloodstream. The activity in other normal organs was negligible in most cases, as confirmed by imaging. Pharmacokinetics data indicated that ^{90}Y-DOTATOC clears slowly from the cavity. The mean τ_{blood} was 0.51 ± 0.18 h (range, 0.25–0.80 h). The cumulative activity curves in the urine increased slowly, confirming that biologic clearance from the tumor cavity is very slow. The mean cumulative activity in the urine was 37 ± 10 %IA up to 48 h after injection; the mean $\tau_{bladder}$ was 0.97 ± 0.23 h considering a bladder voiding interval of 4.8 h. The residence time of ^{90}Y-DOTATOC in the source region was derived from these results and a mean value of τ_{source}, 60 ± 8 h, was obtained.

Dosimetry for ^{90}Y-DOTATOC

The mean absorbed doses ± 1 SD to red marrow, urinary bladder wall, and total body were 0.03 ± 0.01, 1.22 ± 0.27, and 0.006 ± 0.002 mGy/MBq, respectively.

Considering the value of 60 h for τ_{cavity}, we estimated the absorbed dose to the BAT for the different hypotheses regarding radiopharmaceutical distribution.

Figure 3 shows the absorbed dose versus distance from the center of the cavity in case of no binding (geometry 1, hypothesis 1; f = 0), for cavity volumes from 0.5 to
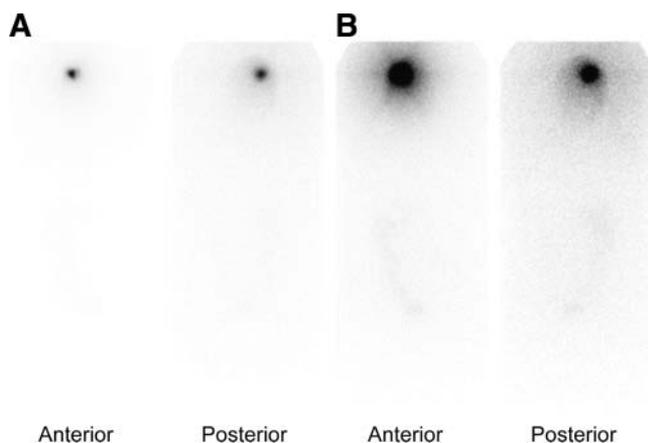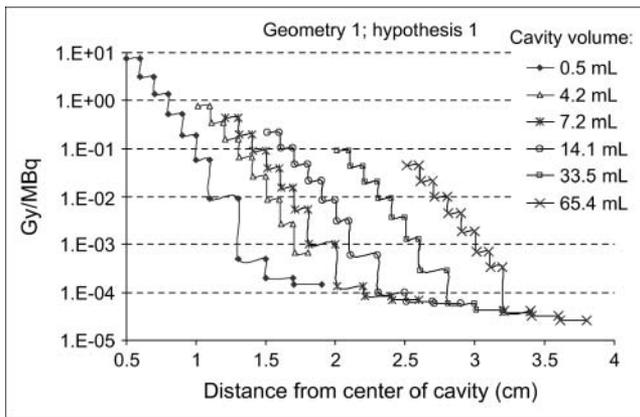
FIGURE 3. Absorbed doses in adjacent subsequent shells for cavities of different volumes (from 0.5 to 65.4 mL), after LR injection of ^{90}Y-DOTATOC in the hypothesis of no binding and no diffusion (geometry 1, hypothesis 1).

FIGURE 5. Absorbed doses for ^{90}Y-DOTATOC in adjacent subsequent shells of a cavity of 7.2 mL, considering 3 different distances of diffusion (geometry 2): 1 mm (continuous line), 3 mm (dashed line), and 6 mm (dotted line) inside the BAT.

65.4 mL. Data are purposely reported in a step-function to express the absorbed doses in subsequent shells of tissue 1-mm thick. The dose in the first few shells decreases considerably as the cavity volume increases and for shell I is 1.0 and 0.116 Gy/MBq for 4.2 and 33.5 mL of SCR volume, respectively. For any fixed volume, the percentage absorbed dose rapidly decreases from the inner to the outer shell reaching at shell VI (6 mm from the edge) <1% of the dose to shell I.

Figure 4 shows the variation of the mean absorbed dose with f values ranging from 0 to 1 (cavity volumes, 0.5–65.4 mL)—combining geometry 1, hypothesis 1 and hypothesis 2—in a target tissue defined as a cuff 6-mm thick surrounding the cavity. Considering a cavity of 7.2 mL, the absorbed doses resulted in 1.7 and 0.2 Gy/MBq for f = 1 (complete binding) and f = 0 (no binding), respectively.

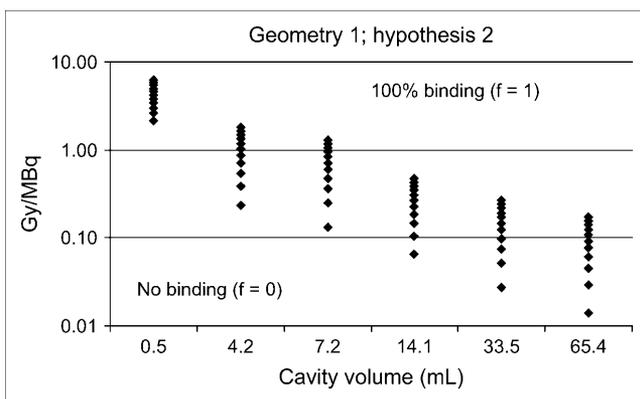Figure 5 shows the absorbed dose versus distance from the center of the cavity (cavity volume, 7.2 mL), consid-

ering a homogeneous diffusion of the radiocompound within a rim of tissue 1-, 3-, and 6-mm thick—geometry 2.

The average absorbed dose to the normal brain was 15 ± 5 μGy/MBq. The absorbed doses to the non-target regions of the head were negligible and are given in Table 3.

Toxicity

No acute or delayed side effects were observed in the treated patients. The blood tests did not demonstrate any significant alteration of the hematologic, hepatic, and renal parameters. No increase of neurologic deficits was reported.

DISCUSSION

The constant high tendency of malignant gliomas to recur locally justifies local therapeutic approaches such as reoperation, stereotactic radiotherapy, radiosurgery, or interstitial brachytherapy. Clinical experience using more innovative schemes has been reported over the past years (28–30), including local hyperthermia, recombinant toxins, various chemotherapeutic agents, and radiopharmaceuticals.

The advantages of local drug administration consist primarily in the bypass of the blood–brain barrier, the achievement of prolonged local concentrations of the pharmaceutical, and the minimization of systemic toxicity. LR radio-immunotherapy using monoclonal antibodies, labeled with β-emitting radionuclides, has shown several advantages in malignant glioma models, including the possibility of destroying large numbers of antigen-negative tumor cells by the so-called cross-fire effect (10,31,32). Correspondingly, the somatostatin receptor–targeted β-irradiation, conveyed by the octapeptide analog DOTATOC, has shown promising results in the local treatment of low-grade and anaplastic astrocytomas expressing sstr2 and sstr5 (7,33,34). Indeed, LR therapy with radioconjugates performed either after (when recurrence occurs) or before (in an adjuvant setting) conventional radiotherapy requires attention to the possible additive toxic effect. Thus, "targeted brachytherapy" should require an accurate dosimetric evaluation. Different from

FIGURE 4. Mean absorbed doses (Gy/MBq) to BAT region 6-mm thick around the cavity. Results are expressed for a range of cavity volumes (horizontal range) and degree of binding to cavity wall for ^{90}Y-DOTATOC (vertical range): from lack of binding (all radiopharmaceutical remains uniformly distributed inside the cavity; f = 0) to complete binding (all radiopharmaceutical is bound to the cavity wall; f = 1).
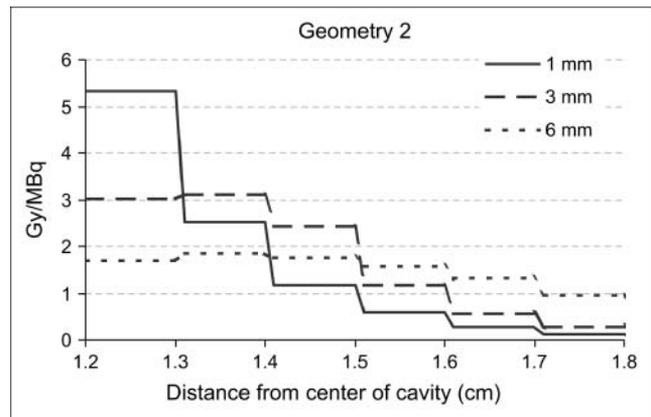
TABLE 3
Absorbed Doses (Mean ± SD) in Different Areas of Head Phantoms (Values Averaged on All Cavity Volumes and Source Distributions) for ^{90}Y-DOTATOC

Region	Absorbed dose (μGy/MBq)
Right eye	5.3 ± 0.9
Left eye	3.3 ± 0.7
Normal brain (right hemisphere)	20.2 ± 9.7
Normal brain (left hemisphere)	8.9 ± 1.0
Skull	13.2 ± 0.7
Right optical nerve	8.3 ± 2.3
Left optical nerve	4.4 ± 1.4

EBRT, in LR radionuclide treatment, dosimetry is strongly time and space dependent. Radiopharmaceuticals may, in fact, show different distribution patterns: molecules can remain inert inside the surgical cavity, they can partially bind to antigens or receptors located on the cell surface facing the cavity wall, and, finally, they can penetrate few millimeters through the BAT.

The first attempts to perform LR therapies were purely clinical and gave information on the absorbed dose to the mere surgical cavity (8,34). Nevertheless, the estimation of the dose inside the cavity, where tumor has been removed and replaced by liquor, does not represent the proper identification of the clinical target. More specific dosimetric approaches are quite limited in the literature and relate primarily to ^{131}I- and ^{90}Y-labeled monoclonal antibodies (13,32,33). A dosimetric approach frequently applied considers the source as incorporated in the cavity wall, well separated from the tumor target. The target is identified as a slice of brain, as thick as the range of the radionuclide under consideration (typically, the R_{95} value [R_{95} is the distance within which the β-particles of ^{131}I and ^{90}Y transfer 95% of their energy] is 0.99 mm for ^{131}I and 5.9 mm for ^{90}Y). With this hypothesis, the authors provide the dose averaged on the whole BAT as the estimate of the absorbed dose to the target.

In our opinion, this particular source–target geometry, though commonly accepted, does not exactly reflect the variation of energy absorption in function of the distance and the real diffusion of radioactive molecules through tissues. Moreover, these models do not take into account the diffusion of different radiocompounds into the BAT. Although acceptable with large monoclonal antibody molecules, this approximation does not seem to apply to radiopeptides, which are smaller molecules showing a distribution gradient through the BAT (33).

With this in mind, our intent was to develop a flexible model, able to estimate the dose by taking into account the variability of source and target geometry. The model was based on the assumption of a homogeneous distributed activity in source, either cavity or progressively surrounding shells (1- to 2-mm thick), into which the BAT has been divided.

We are aware that the availability of biopsy tissue samples, showing the exact degree of molecular binding within the BAT, would offer the proper input data for this model. Unfortunately, we have not been able to obtain such samples in our series of patients.

However, some authors have performed autoradiography after intratumoral injection of ^{90}Y-labeled monoclonal antibodies, by examining radial sections, obtained from open biopsies of the cavity wall (35). Their data indicated a moderate degree of diffusion of antibody conjugates into the brain parenchyma, with a relatively uniform diffusion around the cavity. Despite the limited number of their patients, the results can foster reasonable assumptions on the kinetics of molecules through the tissue.

The algorithm that we developed allows a patient-specific dosimetric evaluation, combining the dimension of the cavity, the degree of radiopharmaceutical binding to the cells, and the percolation into the BAT, as individual parameters.

The main limitation of our study relies on the assumption of an ideal situation, when the SRC is regularly spheric, tumor residual is uniformly distributed in surrounding shells, and radioactivity is homogeneously distributed in the width of tissue. However, for approximately spheric cavities and tumor shells of tissue thicker than 1 mm, the model certainly represents a considerable improvement in dosimetric analysis and offers a reliable estimate.

The rationale of treating anaplastic astrocytoma with peptide receptor radionuclide therapy with ^{90}Y-DOTATOC is based on autoradiographic studies demonstrating a high density of sstr2–sstr5 in this tumor (34). The feasibility and tolerability of LR therapy with ^{90}Y-DOTATOC has been described elsewhere (36).

The LR approach, whenever feasible, guarantees a higher irradiation of the tumor residual cells, while sparing normal organs. At our institute, LR therapy with ^{90}Y-conjugates, both peptides and biotin, has been performed, including a series of patients with recurrent high-grade gliomas. Locally injected activity varied in patient groups and the maximum tolerated dose was defined as the value of 1.1 GBq of ^{90}Y. In 12 compliant patients, dosimetry was performed.

The radioconjugate was shown to clear slowly from the injection site, resulting in a high and stable %IA value in the source region and in a low-activity concentration in the blood. The biokinetic parameters did not differ consistently among patients. Combining the obtained S values with the experimental data of ^{90}Y-DOTATOC, we explored the variation of the absorbed doses among the different shells (1–2 mm) into which the BAT was divided. The results showed a steep gradient as the distance from the cavity increases (the S values for shell VI resulted typically in ~1% of that of shell I). Figures 3 and 5 show that the dose decreases considerably in the subsequent shells for ^{90}Y-DOTATOC.

Overall, our results emphasize the role played by the dimension of the cavity, the diffusion throughout the BAT, and the binding of the ^{90}Y-conjugates in the dose released.

The normal brain is the critical organ for EBRT, as it is inevitably included in the field of treatment. On the contrary, during LR therapy, the normal brain (including optical

nerves and pituitary) received negligible doses (mean dose, 16.5 mGy), at least at a distance longer than the maximum range of ^{90}Y from the cavity wall. Other normal organs potentially at risk, such as red marrow and kidneys (critical organs for systemic ^{90}Y-DOTATOC therapy), also received negligible doses. Therefore, there is enough evidence, supported by dosimetry, that with LR administration, it is possible to deliver very high doses to the tumor, while sparing normal organs and tissues.

These results represent the basis for future prospective trials, considering therapeutic administrations tailored on activity concentration (MBq/mL), instead on a fixed activity.

To date, LR therapy represents an approach performed in few centers, and its emerging role in controlling high-grade gliomas is not yet included in standard clinical protocols (30). In our opinion, future perspectives must include LR therapies, not only as the last therapeutic chance in the final phase of the disease but also as an anticipated boost before EBRT.

For the moment, we can speculate that the ideal timing to perform LR treatment is the interval between surgery and EBRT. Because it is well tolerated, the catheter could be inserted even during the first surgical intervention. The 2- to 4-wk interval, between surgery and external radiotherapy, could be a suitable period to start LR therapy, which could contribute to killing residual tumor cells, thus increasing the disease-free interval.

Recent studies based on the radiobiologic effect depending on radiation and target tissue, suggested considering the biologic effective dose (BED) as a more proper parameter to interpret dose–effect correlation (37–39). In the future, if biologic parameters, such as proliferating time, radiosensitivity, and sublethal damage repair, will be available for high-grade gliomas, combined EBRT and LR protocols could be fine tuned on the basis of the individual preset BED.

CONCLUSION

This model, although not completed with ex vivo microscopic analysis in our patients, represents the basis for further improvements in dosimetry of LR-targeted radionuclide therapies. New clinical protocols of LR radioimmunotherapy in glioblastoma (PAGRIT: Pretargetted Antibody Guided Radioimmunotherapy [Sigma Tau]) and peptide–receptor radiometabolic therapy in anaplastic astrocytomas (^{90}Y-DOTATOC) are beginning to be used. The possibility of tailoring the LR treatment on the individual characteristics of the patient, as presented, will possibly improve the safety and the efficacy of the therapy.

REFERENCES

1. Stewart LA. Chemotherapy in adult high-grade glioma: a systematic review and meta-analysis of individual patient data from 12 randomised trials. *Lancet.* 2002;359:1011–1018.
2. Wong ET, Hess KR, Gleason MJ, et al. Outcomes and prognostic factors in recurrent glioma patients enrolled onto phase II clinical trials. *J Clin Oncol.* 1999;17:2572–2578.
3. Larson DA. Wara WM. Radiotherapy of primary malignant brain tumors. *Semin Surg Oncol.* 1998;14:34–42.
4. Goldenberg DM. Targeted therapy of cancer with radiolabeled antibodies. *J Nucl Med.* 2002;43:693–713.
5. Zalutsky MR. Targeted radiotherapy of brain tumours. *Br J Cancer.* 2004;90:1469–1473.
6. Paganelli G, Bartolomei M, Ferrari M, et al. Pre-targeted locoregional radioimmunotherapy with ^{90}Y-biotin in glioma patient: phase I study and preliminary therapeutic results. *Cancer Biother Radiopharm.* 2001;16:227–235.
7. Merlo A, Hausmann O, Wasner M, et al. Locoregional regulatory peptide receptor targeting with the diffusible somatostatin analogue ^{90}Y-labeled DOTA^0-D-Phe^1-Tyr^3-octreotide (DOTATOC): a pilot study in human gliomas. *Clin Cancer Res.* 1999;5:1025–1033.
8. Riva P, Franceschi G, Riva N, et al. Role of nuclear medicine in the treatment of malignant gliomas: the locoregional radioimmunotherapy approach. *Eur J Nucl Med.* 2000;27:601–609.
9. Buscombe JR, Pigott K. New approaches in targeting intracerebral tumours with ^{90}Y-labelled radiopeptides. *Eur J Nucl Med Mol Imaging.* 2002;29:1697–1698.
10. Hopkins K, Chandler C, Bullimore J, et al. A pilot study of the treatment of patients with recurrent malignant gliomas with intratumoral yttrium-90 radioimmunoconjugates. *Radiother Oncol.* 1995;34:121–134.
11. Carnemolla B, Castellani P, Ponassi M, et al. Identification of a glioblastoma-associated tenascin-C isoform by a high affinity recombinant antibody. *Am J Pathol.* 1999;154:1345–1352.
12. Hofer S, Eichhorn K, Freitag P et al. Successful diffusible brachytherapy (dBT) of a progressive low-grade astrocytoma using the locally injected peptidic vector and somatostatin analogue [^{90}Y]-DOTA^0-D-Phe^1-Tyr^3-octreotide (DOTATOC). *Swiss Med Wkly.* 2001;131(43–44):640–644.
13. Hopkins K, Papanastassiou V, Zananiri FA, et al. A model to estimate the dose to tumor following intracavity administration of radioimmunoconjugates to patients with malignant gliomas. *Br J Radiol.* 1997;70:1152–1161.
14. Snyder WS, Ford MR, Warner GG, et al. MIRD Pamphlet No. 11. *"S" Absorbed Dose per Unit Cumulated Activity for Selected Radionuclides and Organs.* New York, NY: Society of Nuclear Medicine; 1975.
15. Stabin MG, Siegel JA. Physical models and dose factors for use in internal dose assessment. *Health Phys* 2003;85:294-310.
16. Fassò A, Ferrari A, Ranft J, et al. *An Update About FLUKA Proceedings of the 2nd Workshop on Simulating Accelerator Radiation Environments: CERN Report TIS-RP/97-05.* In: Stevenson GR, ed. CERN: Geneva, Switzerland, October 9–11, 1995:158–170.
17. International Commission on Radiation Units and Measurements. *Dosimetry of External Beta Rays for Radiation Protection. ICRU Report 56.* Bethesda, MD: ICRU Publications; 1997.
18. International Commission on Radiological Protection. *Reference Man: Anatomical, Physiological and Metabolic Characteristics. ICRP Publication 23.* Oxford, U.K.: Pergamon Press; 1976.
19. International Commission on Radiation Units and Measurements. *Phantom and Computational Models in Therapy, Diagnosis and Protection. ICRU Report 48.* Bethesda, MD: ICRU Publications; 1992.
20. Torsen, Moller B, Reif E. *Pocket Atlas of Cross-Sectional Anatomy: CT and MRI.* Vol I. Stuttgart, Germany: Thieme Medical Publishers, Inc.; 2000.
21. Robbins SL, Lottrum RS, eds. *Pathologic Basis of Disease.* Philadelphia, PA: Saunders; 1979:1568.
22. Bakker WH, Albert R, Bruns C, et al. [^{111}In-DTPA-D-Phe^1]-octreotide, a potential radiopharmaceutical for imaging of somatostatin receptor-positive tumors: synthesis, radiolabeling and in vitro validation. *Life Sci.* 1991;49:1583–1591.
23. Cremonesi M, Ferrari M, Zoboli S, et al. Biokinetics and dosimetry in patients administered with ^{111}In-DOTA-Tyr^3-octreotide: implications for internal radiotherapy with ^{90}Y-DOTATOC. *Eur J Nucl Med.* 1999;26:877–886.
24. Stabin MG. MIRDOSE: personal computer software for internal dose assessment in nuclear medicine. *J Nucl Med.* 1996;37:538–546.
25. Thomas SR, Stabin MG, Chen CT, et al. MIRD Pamphlet No. 14: a dynamic urinary bladder model for radiation dose calculations. *J Nucl Med.* 1992;33:783–802.
26. Papanastassiou V, Pizer BL, Chandler CL, et al. Pharmacokinetics and dose estimates following intrathecal administration of ^{131}I-monoclonal antibodies for the treatment of central nervous system malignancies. *Int J Radiat Oncol Biol Phys.* 1995;31:541–552.
27. Behr TM, Behe M, Sgouros G. Correlation of red marrow radiation dosimetry with myelotoxicity: empirical factors influencing the radiation-induced myelotoxicity of radiolabeled antibodies, fragments and peptides in pre-clinical and clinical settings. *Cancer Biother Radiopharm.* 2002;17:445–464.

28. Rand RW, Kreitman RJ, Patronas N, et al. Puri RK. Intratumoral administration of recombinant circulatory permuted interleukin-4-Pseudomonas exotoxin in patients with high-grade glioma. *Clin Cancer Res.* 2000;6:2157–2165.

29. Barba D, Saris SC, Holder C, Rosenberg SA, Oldfield EH. Intratumoral LAK cell and interleukin-2 therapy of human gliomas. *J Neurosurg.* 1989;70: 175–182.

30. Boiardi A, Salmaggi A, Pozzi A, et al. Interstitial chemotherapy with mitoxantrone in recurrent malignant glioma: preliminary data. *J Neurooncol.* 1996;27: 157–162.

31. Riva P, Franceschi G, Frattarelli M. Loco-regional radioimmunotherapy of high-grade malignant gliomas using specific monoclonal antibodies labeled with ^{90}Y: a phase I study. *Clin Cancer Res.* 1999;5(suppl):3275s–3280s.

32. Cokgor I, Akabani G, Kuan CT. Phase I trial results of iodine-131-labeled antitenascin monoclonal antibody 81C6 treatment of patients with newly diagnosed malignant gliomas. *J Clin Oncol.* 2000;18:3862–3872.

33. Merlo A, Mueller-Brand J, Maecke HR. Comparing monoclonal antibodies and small peptidic hormones for local targeting of malignant gliomas. *Acta Neurochir Suppl.* 2003;88:83–91.

34. Reubi JC, Horisberger U, Lang W, Koper JW, Braakman R, Lamberts SWJ. Coincidence of EGF receptor and somatostatin receptors in meningiomas but inverse, differentiation-dependent relationship in glial tumors. *Am J Pathol.* 1989;134:337–344.

35. Hopkins K, Chandler C, Eatough J, Moss T, Keamshead JT. Direct injection of ^{90}Y MoAbs into glioma tumor resection cavities leads to limited diffusion of the radioimmunoconjugates into normal brain parenchyma: a model to estimate absorbed radiation dose. *Br J Radiat Oncol Biol Phys.* 1998;40:835–844.

36. Schumacher T, Hofer S, Eichhorn K, et al. Local injection of the ^{90}Y-labelled peptidic vector DOTATOC to control gliomas of WHO grades II and III: an extended pilot study. *Eur J Nucl Med Mol Imaging.* 2002;29:486–493.

37. Dale R. Dose-rate effects in targeted radiotherapy. *Phys Med Biol.* 1996;41: 1871–1884.

38. Dale R. Use of the linear-quadratic radiobiological model for quantifying kidney response in targeted radiotherapy. *Cancer Biother Radiopharm.* 2004;19: 363–370.

39. Kassis AI, Adelstein SJ. Radiobiologic principles in radionuclide therapy. *J Nucl Med.* 2005;46(suppl):4S–12S.